

Determination of ground conductivity and system parameters for optimal modeling of geomagnetically induced current flow in technological systems

Antti Pulkkinen^{1,2}, Risto Pirjola^{3,4}, and Ari Viljanen³

¹Goddard Earth Sciences and Technology Center, University of Maryland, Baltimore, Maryland, USA

²NASA/GSFC, Greenbelt, Code 674, MD 20771, USA

³Space Research Unit, Finnish Meteorological Institute, Helsinki, Finland

⁴Geomagnetic Laboratory, Geological Survey of Canada, Natural Resources Canada, Ottawa, Ontario, Canada

(Received January 22, 2007; Revised June 13, 2007; Accepted August 10, 2007; Online published September 28, 2007)

In this work, methods to determine technological system parameters and the ground conductivity structure from different sets of geomagnetically induced current (GIC), magnetic field and geoelectric field observations are explored. The goal of the work is to enable optimal modeling of induced currents in any technological system experiencing GIC. As an additional product, the introduced methods can also be applied to utilize GIC observations in the imaging of the subsurface geological structures. Here a robust processing scheme and Occam's inversion technique familiar from magnetotelluric (MT) studies are applied to the determination of the ground conductivity structure. The application of the methods to GIC data from the Finnish pipeline for a storm period of October 24–November 1, 2003 demonstrate that optimal system parameters and ground conductivity structure can be obtained using time series comprising only 8 days worth of data. Importantly, the obtained ground model is in agreement with models obtained in earlier MT studies. Furthermore, it is shown that although in an ideal case the magnetic field data used should be obtained from the immediate vicinity of the GIC observation site, some spatial separation (200–300 km) between the sites can be tolerated.

Key words: Geomagnetic induction, geomagnetically induced currents, GIC, modeling, inversion, space weather.

1. Introduction

Geomagnetically induced currents (GIC) flowing in long conductor systems at the surface of the Earth are a ground manifestation of complex dynamical processes in the Earth's near-space. GIC are not only of scientific interest but via their effects on technologies, such as power transmission systems and oil and gas pipelines (e.g. Boteler *et al.*, 1998; Pirjola, 2002), they are also a subject of very practical interest. It follows that the pursuit of optimal modeling of the GIC phenomenon has a two-fold objective: firstly, to gain physical understanding about our near-space and subsurface environments and processes associated with the geomagnetic induction phenomenon, and secondly, to obtain practical means to estimate the GIC flows in specific technological systems to evaluate and perhaps to mitigate the societal effects of the phenomenon.

It is well-established that if one has knowledge about the topology and electrical parameters of the technological system (called hereafter collectively as system parameters) under investigation and about the subsurface conductivity structure and ground magnetic field variations, GIC can be modeled in the most common situations (typically effectively one-dimensional Earth) quite accurately (e.g. Pulkki-

nen *et al.*, 2001a; Viljanen *et al.*, 2006). However, information about the optimal GIC modeling setup is often not directly available and, thus, some alternative means to derive the setup is needed. Accordingly, the goal of this work is to explore methods that can be used to derive the optimal system parameters and the conductivity structure from different sets of recordings of GIC, ground magnetic field fluctuations and the geoelectric field.

GIC observations are a poorly utilized data source in magnetotelluric (MT) investigations in which the ground conductivity structure is imaged by means of electromagnetic methods. Although geoelectric potential difference recordings from, for example, submarine cables have been often used in MT studies (see Utada *et al.*, 2003), to our knowledge, the only earlier attempts to use GIC or pipe-to-soil potential observations in MT studies have been made by Brasse and Junge (1984), Pal'shin (1998) and McKay (2003). GIC observations are more and more commonly carried out around the globe in the context of space weather, and many of the GIC time series are long: Finnish pipeline GIC measurements have been carried out continuously with a 10-s cadence since November 1998. GIC observations thus provide a valuable source of additional information usable in MT-based studies. The usage of GIC data in MT studies is explored both theoretically and in terms of practical examples in this work.

The structure of the paper is as follows. First, in Sec-

Copyright © The Society of Geomagnetism and Earth, Planetary and Space Sciences (SGEPSS); The Seismological Society of Japan; The Volcanological Society of Japan; The Geodetic Society of Japan; The Japanese Society for Planetary Sciences; TERRAPUB.

tion 2 we explore means to extract the system parameters using two different sets of observations: (1) GIC and the geoelectric field and (2) GIC and horizontal components of the ground magnetic field. In Section 3 we assume that the system parameters are known and proceed to derive a ground conductivity model consistent with the GIC and the ground magnetic field observations. Finally, in Section 4 we briefly discuss our findings and explain how the introduced methods can be applied to particular sets of observations.

2. Determination of the System Parameters

In this section we describe two different means to extract the system parameters from GIC, magnetic field and geoelectric field observations. One should note that system parameters can be determined for discretely and continuously grounded systems without observational data by using GIC computation methods developed by Lehtinen and Pirjola (1985) and Pulkkinen *et al.* (2001a). However, often the technical information needed for such computations is not available, or it is more practical to fit parameters to observations.

Usually, GIC at a site can be modeled to a good approximation by a simple formula

$$GIC(t) = aE_x(t) + bE_y(t) + \epsilon(t) \quad (1)$$

where E_x and E_y are the horizontal components of the local geoelectric field, a and b are the site-dependent system parameters which depend on the topology and the electrical characteristics of the system under investigation and t denotes time. In another words, system parameters define the response of a particular site experiencing GIC to the driving geoelectric field. In practical applications, there is always noise present and, consequently, we have included also the noise term $\epsilon(t)$ to Eq. (1). In the absence of noise, Eq. (1) without the noise term holds exactly if the driving geoelectric field is uniform (e.g. Pulkkinen *et al.*, 2006b) and the temporal variations are quasi-dc, i.e. there is no inductive coupling between the system and the geoelectric field. It is shown by Viljanen *et al.* (2004) that Relation (1) holds approximately also for non-uniform sources if the meso-scale (~ 100 km) geoelectric field in the immediate vicinity of the GIC-site of interest is known. Generally speaking, this means that a and b are dominated by the local properties, i.e. the geometry including the orientation and the electrical dc-resistances of the segment of the network around the site at which the GIC is considered.

We now consider two different settings used to extract information about the system parameters: (1) GIC and the geoelectric field are known, and (2) GIC and the ground magnetic field variations are known. Obviously, the case (2) is the more typical situation in practical applications where neither the system parameters nor the ground conductivity structure are known. However, if the geoelectric field is known, via direct measurements or modeling by using the known ground conductivity structure, we can extract a and b from Eq. (1). Although a and b could in principle be solved from two independent observations at times t_1 and t_2 , to facilitate the entire time series, we multiply Eq. (1) by $E_x(t)$ and $E_y(t)$ and compute the expectation to obtain

$$\langle GIC(t)E_x(t) \rangle = a \langle E_x(t)^2 \rangle + b \langle E_y(t)E_x(t) \rangle + \langle \epsilon(t)E_x(t) \rangle \quad (2)$$

$$\langle GIC(t)E_y(t) \rangle = a \langle E_x(t)E_y(t) \rangle + b \langle E_y(t)^2 \rangle + \langle \epsilon(t)E_y(t) \rangle \quad (3)$$

where $\langle \cdot \rangle$ denotes the expectation taken over different realizations of the process. Note that in a general non-stationary case, for example, $\langle E_x(t)^2 \rangle$ depends on t . We then assume that the noise $\epsilon(t)$ has zero mean and is statistically independent of the geoelectric field. We note that although these are standard assumptions used frequently, for example, in magnetotelluric studies, especially the assumption about the independence may not always hold. However, detailed investigation of the matter is beyond the scope of this work. Instead, we argue that since the methods developed here are seen to clearly improve the GIC modeling accuracy, the assumptions made are at least to some degree justified. Thus, assuming zero mean of the noise and the independence between the noise and the geoelectric field, from Eqs. (2) and (3) we can solve

$$a = \frac{\langle GIC E_y \rangle \langle E_x E_y \rangle - \langle GIC E_x \rangle \langle E_y^2 \rangle}{\langle E_x E_y \rangle^2 - \langle E_x^2 \rangle \langle E_y^2 \rangle} \quad (4)$$

$$b = \frac{\langle GIC E_x \rangle \langle E_x E_y \rangle - \langle GIC E_y \rangle \langle E_x^2 \rangle}{\langle E_x E_y \rangle^2 - \langle E_x^2 \rangle \langle E_y^2 \rangle} \quad (5)$$

where we have assumed stationarity of the time series and have thus dropped the explicit temporal dependence.

If only GIC and the horizontal ground geomagnetic variations are known, only the ratio b/a can be determined. To show this, we first express the geoelectric field in the spectral domain as

$$\tilde{E}_{x,y} = \pm \frac{\tilde{Z}}{\mu_0} \tilde{B}_{y,x} + \tilde{\epsilon}' \quad (6)$$

where μ_0 is the vacuum permeability, \tilde{B}_x and \tilde{B}_y denote the horizontal components of the magnetic field and \tilde{Z} is the surface impedance, tilde denotes quantities in the spectral domain and the 1D assumption enables the usage of just the off-diagonal components of the surface impedance tensor which relates the ground horizontal magnetic field to the corresponding electric field in the frequency domain (Cagniard, 1953). $\tilde{\epsilon}'$ in Eq. (6) is the noise term. In expressing the geoelectric field via Eq. (6), we also assume that the variations of the horizontal geomagnetic field are linear with respect to the x and y coordinates (Dmitriev and Berdichevsky, 1979) in the spatial scales (~ 100 km) considered. By using Eq. (6) we then express Eq. (1) in the spectral domain as

$$\tilde{GIC} = \frac{a}{\mu_0} \tilde{Z} \tilde{B}_y - \frac{b}{\mu_0} \tilde{Z} \tilde{B}_x + (a-b) \tilde{\epsilon}' + \tilde{\epsilon} \quad (7)$$

Equation (7) is then multiplied by \tilde{B}_x^* and \tilde{B}_y^* (asterisk denotes a complex conjugate) to obtain

$$\tilde{GIC} \tilde{B}_x^* - \tilde{\epsilon}'' \tilde{B}_x^* = \frac{a}{\mu_0} \tilde{Z} \tilde{B}_y \tilde{B}_x^* - \frac{b}{\mu_0} \tilde{Z} \tilde{B}_x \tilde{B}_x^* \quad (8)$$

$$\tilde{GIC} \tilde{B}_y^* - \tilde{\epsilon}'' \tilde{B}_y^* = \frac{a}{\mu_0} \tilde{Z} \tilde{B}_y \tilde{B}_y^* - \frac{b}{\mu_0} \tilde{Z} \tilde{B}_x \tilde{B}_y^* \quad (9)$$

where $\tilde{\epsilon}''$ is the combined noise term from the right-hand side of Eq. (7). From Eqs. (8) and (9) we can then solve

$$c \equiv \frac{b}{a} = \frac{\tilde{B}_y \tilde{B}_x^* - \chi |\tilde{B}_y|^2}{|\tilde{B}_x|^2 - \chi \tilde{B}_x \tilde{B}_y^*} \quad (10)$$

where

$$\chi = \frac{\tilde{GIC} \tilde{B}_x^* - \tilde{\epsilon}'' \tilde{B}_x^*}{\tilde{GIC} \tilde{B}_y^* - \tilde{\epsilon}'' \tilde{B}_y^*} \quad (11)$$

To obtain the above formulation in the temporal domain, we assume stationarity of the signals and use the cross-correlation theorem to give, for example,

$$\tilde{B}_y \tilde{B}_x^* = \frac{1}{\sqrt{2\pi}} \int_{-\infty}^{\infty} \langle B_y B_x \rangle [\tau] e^{-i\tau\omega} d\tau \quad (12)$$

where ω is the angular frequency and where

$$\langle B_y B_x \rangle [\tau] = \int_{-\infty}^{\infty} B_y(t) B_x(t - \tau) dt \quad (13)$$

Since we are looking for a solution of c which is independent of the frequency, i.e. we may assume that $\omega = 0$, we can express c in Eq. (10) using the correlation functions in the temporal domain as

$$c = \frac{\int_0^{\infty} \langle B_y B_x \rangle [\tau] d\tau - \chi' \int_0^{\infty} \langle B_y B_y \rangle [\tau] d\tau}{\int_0^{\infty} \langle B_x B_x \rangle [\tau] d\tau - \chi' \int_0^{\infty} \langle B_x B_y \rangle [\tau] d\tau} \quad (14)$$

where we have assumed that the correlation functions are symmetric around $\tau = 0$ and where

$$\chi' = \frac{\int_0^{\infty} \langle GIC B_x \rangle [\tau] d\tau - \int_0^{\infty} \langle \epsilon'' B_x \rangle [\tau] d\tau}{\int_0^{\infty} \langle GIC B_y \rangle [\tau] d\tau - \int_0^{\infty} \langle \epsilon'' B_y \rangle [\tau] d\tau} \quad (15)$$

To further simplify the method, we assume that the functional form of the correlation functions is identical. For example,

$$\langle B_y B_x \rangle [\tau] = \langle B_y B_x \rangle [\tau = 0] G(\tau) \quad (16)$$

where function G , which is assumed to be common for all correlation functions in Eq. (14), is some function of τ . Also, we assume that the combined noise term ϵ'' has zero mean and is statistically independent of both B_x and B_y . Then, Eq. (14) reduces to

$$c = \frac{\langle B_y B_x \rangle - \chi'' \langle B_y B_y \rangle}{\langle B_x B_x \rangle - \chi'' \langle B_x B_y \rangle} \quad (17)$$

where

$$\chi'' = \frac{\langle GIC B_x \rangle}{\langle GIC B_y \rangle} \quad (18)$$

It should be noted that the correlation functions in Eqs. (17) and (18) need to be evaluated only at $\tau = 0$.

Although the formulation above was made using B_x and B_y , via identity

$$\tilde{B}_{x,y} = \frac{1}{i\omega} \frac{d\tilde{B}_{x,y}}{dt} \quad (19)$$

the formulation can be carried out identically also for the time derivative of the horizontal magnetic field dB_x/dt and

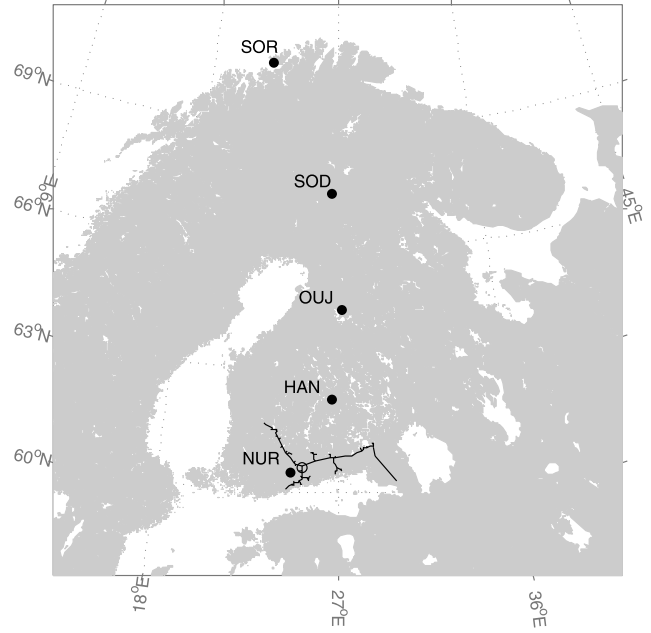


Fig. 1. The locations of IMAGE stations NUR, HAN, OUJ, SOD and SOR (black dots) and the GIC measurement site at Mäntsälä (circle). The black curve shows the route of the Finnish pipeline. Geographic coordinates are used.

dB_y/dt : in Eqs. (17) and (18) one just makes replacements $B_x \rightarrow dB_x/dt$ and $B_y \rightarrow dB_y/dt$. The evaluation of the expressions above at $\omega = 0$ is not a problem since the “extra” ω s introduced by replacement (19) cancel out from Eqs. (10) and (11). In fact, the usage of time derivatives of the magnetic field is preferred because of their shorter characteristic correlation times and roughly exponentially decaying functional form of the function G (not shown here) validating, at least partially, the assumption about common G made to arrive at Eqs. (17) and (18).

To justify the various assumptions made above, we investigate how well the method expressed by Eqs. (17) and (18) (with dB_x/dt and dB_y/dt) performs by using a modeled data set. We use 10-s time resolution geomagnetic data from the Nurmijärvi Geophysical Observatory (NUR) (see Fig. 1) for a storm period of October 24–November 1, 2003 to model the geoelectric field. This specific period is used throughout the paper because it includes, in the context of space weather, the important “Halloween” storm event and the length of the period is long enough from the statistical viewpoint to carry out the investigation in Section 3 to periods up to about ~ 1000 s. The geoelectric field is modeled by applying the plane wave method (e.g. Viljanen *et al.*, 2004) with a ground conductivity model of central Finland (e.g. Viljanen *et al.*, 1999) (the particular choice of the conductivity model is unimportant). We then use various realistic values of a and b to compute 100 data sets of modeled GIC via Eq. (1). The modeled GIC and dB_x/dt and dB_y/dt are then used to determine the ratio c . The results of these computations are shown in Fig. 2, which shows that with this particular modeling setup for large c we underestimate the ratio, and for small c we tend to overestimate it. However, if the difference between a and b is not very large (difference well below an order of magnitude), the method

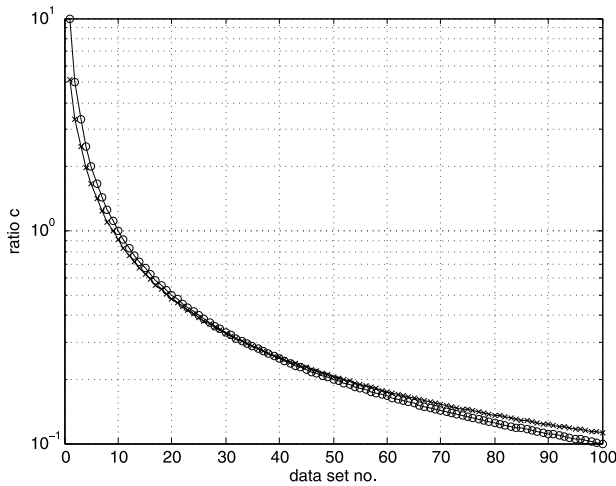


Fig. 2. The original ratio c used in computing the modeled GIC (circles) and c determined using Eqs. (17) and (18) (crosses). See text for details.

is seen to perform quite well, even in its simplest form. We are thus encouraged to apply the method to measured GIC.

The ratio c for the GIC measurements in the Finnish natural gas pipeline (Pulkkinen *et al.*, 2001b) is determined by using 10-s time resolution data for the period of October 24–November 1, 2003. The geomagnetic recordings from NUR, which is located 30 km to the south-west from the GIC measurement site (see Fig. 1), are used as geomagnetic reference data. The analysis of GIC and dB_x/dt and dB_y/dt from NUR based on Eqs. (17) and (18) results in $c = -0.6$. Note that because the determination of c involves ratios, the method is quite sensitive to inaccuracies in the computed correlations. To estimate the level of sensitivity, the above analysis is repeated with an extended data set of Finnish pipeline GIC measurements for the period September 22–November 21, 2003 comprising 60 days of data instead of the 8 days used above. The analysis with extended data gives again $c = -0.6$ (difference between two values of c is in the third decimal), indicating that the determined ratio is likely quite accurate. The robustness of the determined c casts some doubt on the validity of a and b determined for the GIC measurements site from the topology and electrical properties of the pipeline (Pulkkinen *et al.*, 2001b), giving a and b with the ratio $c = -1.3$. Possible explanations for the discrepancy include changes in the pipeline system between 2001 and 2003 and the underestimated effect of smaller branches of the Finnish pipeline. Noise neglected above may also affect the analysis. However, the detailed reason for the discrepancy will be a matter of another study.

Often magnetic field observations are not available from the immediate vicinity of the GIC measurement site. Thus, from the practical application viewpoint, it is of interest to investigate how quickly the estimate in c degrades as the distance between the magnetometer and GIC sites increases. We utilize IMAGE magnetometer array data from stations HAN, OUI, SOD and SOR (see Fig. 1) having distances of 200, 450, 750 and 1112 kilometers to the GIC measurement site, respectively. The analysis above is repeated using magnetic data from each station separately for the period of October 24–November 1, 2003. The obtained

c using data from HAN, OUI, SOD and SOR are -0.5 , -0.5 , -0.2 and -0.1 , respectively. The result is somewhat surprising; considering the highly complex structure of the auroral ionospheric current systems (see Pulkkinen *et al.*, 2006a), we expected the estimated c to degrade very rapidly as a function of distance between GIC and magnetometer sites. However, a good estimate for c is obtained even with a separation of 450 km. This indicates that the spatial correlations of the magnetic field fluctuations are in fact high enough, even in the auroral region during disturbed times, to enable the usage of magnetic field and GIC observation pairs not in the immediate vicinity ($\sim 10\text{--}100$ km) of each other.

3. Determination of the Ground Conductivity Structure

In this section, we will assume that the system parameters a and b in Eq. (1) have been determined, for example using the methods described above, and that the a ground magnetic field variations in the vicinity of the GIC measurement site are known. Then, by assuming a 1D ground conductivity structure we will be able to determine ground model that is consistent with the observations.

We assume that the horizontal variations of the geomagnetic field are linear and use Eq. (7) to find the surface impedance \tilde{Z} by minimizing expression

$$\sum_{\omega} f \left[\tilde{Z} \left(a\tilde{B}_y - b\tilde{B}_x \right) - \mu_0 GIC \right] \quad (20)$$

where the summation is over the frequencies and $f[x]$ is some function of its argument x . In a standard least-squares scheme, the function would be $f[x] = |x|^2$. Note that instead of the *transfer function* between GIC, B_x and B_y determined by McKay (2003), we estimate the *surface impedance*, which allows us to use standard MT techniques to deduce the ground conductivity structure.

The surface impedance (tensor) contains information about the ground conductivity and is the main quantity of interest in, for example, MT sounding investigations of the structures in the Earth's crust and upper mantle (approximately within depths of $1000 \text{ km} > |z| > 100 \text{ m}$). The standard MT procedure involves inversion of the determined surface impedance to a ground conductivity model consistent with some specific features of \tilde{Z} . The optimal determination of \tilde{Z} from the measured time series and the following inversion of \tilde{Z} is quite involved and has been a matter of intense studies since the introduction of the MT method (Tikhonov, 1950; Cagniard, 1953). We will cover here only the basic idea of the steps needed to derive \tilde{Z} and the corresponding ground model; the reader should consult the MT literature for a more detailed information on the subject (e.g. Simpson and Bahr, 2005, and references therein).

The first goal is to derive as reliable as possible surface impedance \tilde{Z} from the measured GIC, B_x and B_y . The data were first pre-whitened and then divided into M partially overlapping segments. Cosine-tapered data in each segment were Fourier-transformed. We then set logarithmically spaced frequency bins and determined data points falling to each bin. If the number of points in the frequency

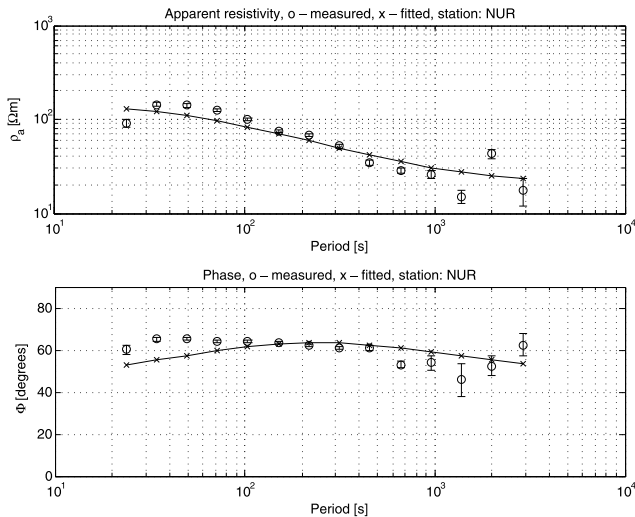


Fig. 3. Circles: the apparent resistivity (top panel) and the phase (bottom panel) computed from the derived surface impedance. Crosses: the apparent resistivity and the phase of the inverted 1D conductivity model. Error bars give the standard error obtained via Bootstrap. GIC observations carried out at Mäntsälä and geomagnetic observations carried out at NUR for the period of October 24–November 1, 2003 were used to derive the surface impedance from which the apparent resistivity and the phase were computed.

bin i is N , we have $M \cdot N$ data points to determine \tilde{Z}_i associated with Eq. (20). It should be noted that a simple straightforward least-squares solution is not appropriate, for example, due to heavy non-Gaussian tails of the residuals (Egbert and Booker, 1986). Thus, here \tilde{Z} was determined using a Robust M-estimator algorithm (Egbert and Booker, 1986; Eisel and Egbert, 2001) that gives less weight for the “bad” data points to avoid a biased estimate. Confidence limits were obtained by Bootstrapping the data (e.g. Press *et al.*, 1992).

We divided the *GIC*, B_x and B_y 10-s data for the period of October 24–November 1, 2003 into 60-min long windows with 50% overlap between the neighbouring windows. The Fourier-transformed data were then sorted into 14 frequency bins, and the corresponding \tilde{Z}_i was determined using the Robust M-estimation. The resulting \tilde{Z}_i was then converted to apparent resistivity $\rho_{a,i}$ and phase Φ_i using formulas

$$\rho_{a,i} = \frac{|\tilde{Z}_i|^2}{\omega\mu_0} \quad (21)$$

$$\Phi_i = \tan^{-1} \left(\frac{\text{Im}(\tilde{Z}_i)}{\text{Re}(\tilde{Z}_i)} \right) \quad (22)$$

where ω is the angular frequency and Im and Re indicate the imaginary and real parts of a complex quantity, respectively. The Bootstrapping was carried out by repeating the analysis 30 times for randomly drawn data (with replacement). Figure 3 shows the obtained $\rho_{a,i}$ and Φ_i , and it is seen that despite the short temporal length of the interval (8 days) used, relatively good estimates are obtained up to a period of about 3000 s.

The inversion of incomplete surface impedance or equivalently apparent resistivity and phase data to a specific

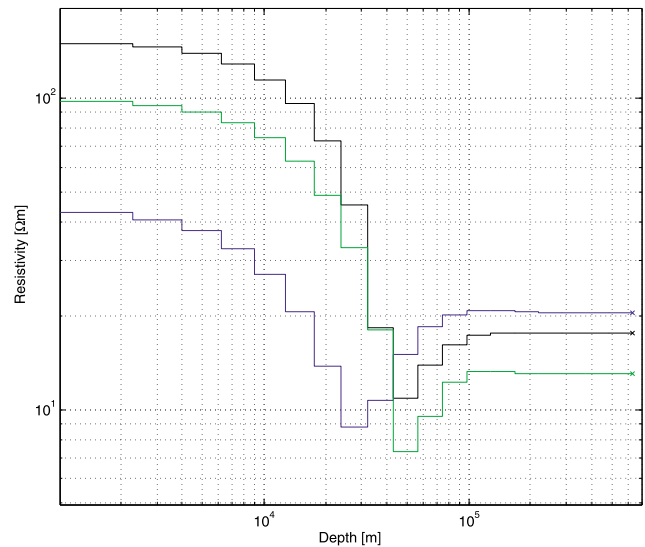


Fig. 4. Ground conductivity models inverted using GIC measurements carried out at Mäntsälä. Black curve: model inverted using magnetic field measurements from NUR, blue curve: model inverted using magnetic field measurements from HAN, green curve: model inverted using magnetic field data for 60 days from NUR (and GIC data from Mäntsälä). The cross denotes the resistivity of the terminating half-space.

ground conductivity model is even in a 1D case a very ill-posed problem (e.g. Weidelt, 1972). Thus, additional *a priori* information/assumptions are needed to stabilize the inversion. One attractive assumption is that the ground is “simple” in terms of the variations of the conductivity as a function of depth. An assumption about such simplicity leads to *Occam’s inversion* (Constable *et al.*, 1987) where the cost function to be minimized is composed of both the model-data residual and the gradients in the ground model. We will use a slightly simplified version of the classical Occam’s inversion algorithm where instead of letting the Lagrange multiplier μ vary as the predefined model-data residual is searched, μ is set to a fixed value. The value of μ determines how much weight is given to individual terms in the cost function: small μ will give better fit to data (more weight on the model-data residual term of the cost function), large μ will give a smoother ground model (more weight on the gradient term). The inversion is terminated once appropriate convergence of the model has been achieved. In practice this was achieved in the inversions below in about 20 iterations.

A simplified 1D Occam’s inversion¹ with weights derived from Bootstrapped confidence limits was used to invert the data in Fig. 3. The initial model used in the inversion was a uniform ground with a resistivity of 10 Ω m and we used $\mu = 0.3$. We modified the coefficients a and b derived by Pulkkinen *et al.* (2001b) to give the ratio c computed above; we chose to set a to value found by Pulkkinen *et al.* (2001b) and to adjust the coefficient b to obtain the desired c . The new coefficients are $a = -70$ A km/V and $b = 40$ A km/V. The obtained ground conductivity

¹Note that the $\frac{\partial \rho_a}{\partial p_j}$ term in the Appendix of Constable *et al.* (1987) needs to be multiplied by a factor 2.

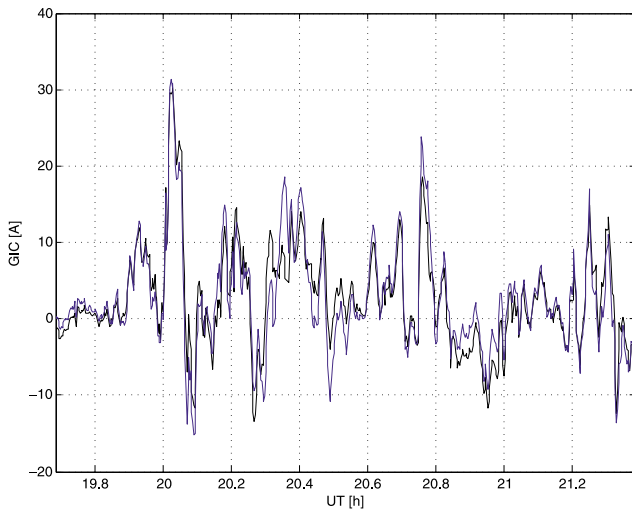


Fig. 5. The measured (black line) and the modeled GIC at Mäntsälä. Time is UT hours from the beginning of July 15, 2000.

model is shown in Fig. 4, and the apparent resistivity and the phase given by the model are depicted in Fig. 3. The model is seen to agree with the observed apparent resistivity and phase quite well. In general, the derived ground model is reasonable, and we see evidence for the existence of a conducting layer at depths of about 30–50 km. Importantly, the same conductor has been indicated in a GIC-based (400 kV transmission line) MT study of the same region by Pal'shin (1998) and also by other standard MT studies (see Korja *et al.*, 2002). The similarity of the derived ground model to ones obtained in earlier MT studies is a clear indication that GIC observations can be used to supplement standard MT data sets.

Finally, to see how well the derived system parameters and the ground model generate the measured GIC, we used the plane wave method to compute the modeled GIC from geomagnetic field observations at NUR for the “Bastille Day” storm event of July 15–16, 2000. From Fig. 5, which shows the measured and modeled GIC, we see that the optimized modeling procedure generates the measured GIC very accurately. We note that in comparison to earlier studies where more simple ground models were used, the layered structure derived here gives a more accurate modeled GIC over the wide frequency band involved with the GIC phenomenon. To investigate the overall improvement in GIC modeling accuracy obtained by the methods introduced here, we also computed GIC by using the system parameters and the ground model for the Finnish pipeline GIC used by Viljanen *et al.* (2006). Viljanen *et al.* (2006) used $a = -70$ A km/V and $b = 88$ A km/V and a two-layer ground with resistivities 38.5Ω m (upper layer) and 0.385Ω m (terminating half-space). We then computed the difference between the modeled and the measured GIC and derived the corresponding error distributions which, are shown in Fig. 6. As is seen, the new system parameters and the ground model provide clear improvement to the modeling accuracy: the number of large errors is especially greatly reduced. We also computed relative errors defined as $(\text{GIC}_{\text{measured}} - \text{GIC}_{\text{modeled}})/\text{GIC}_{\text{measured}}$ for both modeled

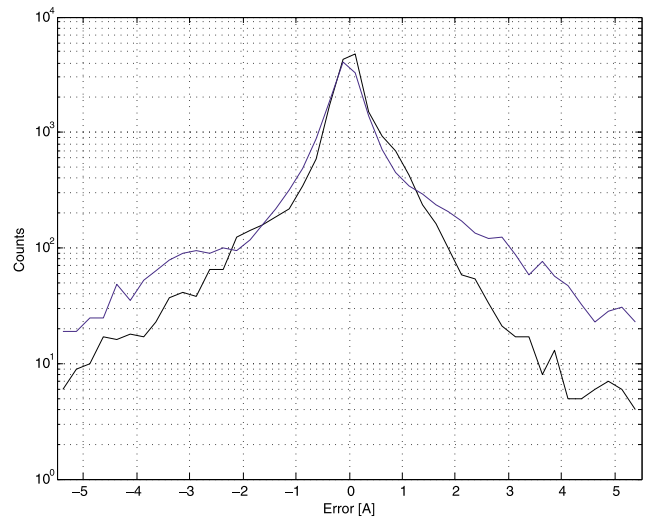


Fig. 6. Error distributions for modeled GIC ($\text{GIC}_{\text{measured}} - \text{GIC}_{\text{modeled}}$). Blue curve shows the distribution for GIC modeled using the system parameters and the ground model by Viljanen *et al.* (2006) and the black curve shows the distribution for GIC modeled using the system parameters and the ground model derived here.

GIC to enable direct comparisons to model validation results presented by Viljanen *et al.* (2006). Only values corresponding to $|\text{GIC}_{\text{measured}}| > 1$ A were used in the analysis. The relative error also shows a clear improvement: median error of the modified model setup is 35% while the model used by Viljanen *et al.* (2006) gives a median error of 59% for the used event.

As previously highlighted, often there are no magnetic field observations available from the immediate vicinity of the GIC measurement site. Thus, it is of interest to investigate how quickly the derived ground model becomes unreliable when the distance between the GIC and magnetometer sites increases. We again utilized IMAGE magnetometer array data from stations HAN, OUI, SOD and SOR. The computations were repeated using magnetic data from each station separately for the period of October 24–November 1, 2003. In addition, to investigate the effect of the relatively short time series used to derive the ground model, we repeated the computations with data from NUR for the 60-day period of September 22–November 21, 2003. The results of the inversions are shown in Fig. 4. It is seen that though the model obtained by using 8 days of data is slightly more conductive, the models derived using 8 and 60 days of data from NUR are very similar: 8 days of data from geomagnetically active period is in this case enough to build an optimal ground model for GIC calculations. The ground model derived using data from HAN deviates from the NUR models. Namely, there is a systematic bias toward higher conductivities at smaller depths which most likely results from the higher amplitudes of the magnetic field variations at HAN: higher conductivity is required to generate the same GIC. However, the correlation coefficient between the measured GIC and the GIC calculated using the HAN ground model and HAN geomagnetic data for October 24–November 1, 2003 is 0.7 which can be considered satisfactory in the context of complex geophysical signals. The surface impedances derived using data from OUI, SOD

and SOR did not give well-converging inversions, which indicates that the 450-km distance between the GIC and magnetometer sites is too large in the geomagnetic and geological conditions in question.

4. Discussion and Conclusions

In this work we have explored methods that can be used to extract values of the system parameters and a 1D ground conductivity structure from different sets of recordings of GIC, ground magnetic field and geoelectric field; the goal was to enable optimal modeling of GIC flow in technological systems. It was seen that the optimization can be approached in a number of different ways, each of which make various assumptions about the GIC phenomenon. It is quite clear that the validity of these assumptions cannot always be justified. Examples of such situations include steep lateral ground conductivity gradients, for example, at the ocean-continent boundaries violating the 1D assumption and the usage of very short time series when stationarity of the GIC signal cannot be assumed even in an average sense. However, our examples show that satisfactory results are obtainable at a geologically complex—i.e. three-dimensional—region of southern Finland (Korja *et al.*, 2002) and with a relatively short time series comprising only 8 days of data. Part of the validity of the 1D assumption results from the spectral characteristics of the GIC phenomenon; most of the power of GIC fluctuations are concentrated in frequencies which penetrate to depths where the ground is to a good approximation 1D (see also Pulkkinen and Engels, 2005). Furthermore, the random noise-like character of both GIC and the time derivative of the ground magnetic field (Pulkkinen *et al.*, 2006a) renders signals both more stationary and spatially smooth on average.

Let us then give a specific example on the usage of the methods described above. We assume a typical situation in which GIC is measured at some part of the technological system and that we have recordings of magnetic field fluctuations from the vicinity of the GIC site. “Vicinity” in the case of the auroral region was seen to be less than about 200–300 km. Note that at lower latitudes where the source field is more uniform, the “vicinity” can cover larger distances (e.g. Koen, 2002; Hejda and Bochnicek, 2005). One then sets a baseline for the response of the system to a given geoelectric field, i.e. one needs to estimate a value for either coefficient a or b in Eq. (1). Note that while the accuracy of the baseline estimate is very important for using GIC measurements as means to image the ground conductivity structure, it is not important in generating an optimal model for GIC computations. More specifically, possible inaccuracies in estimating the baseline value will be absorbed by a static shift in the determined apparent resistivity and resulting ground model. Also, note that if the geoelectric field is known, we can use Eqs. (4) and (5) to solve both a and b directly from the observations. After setting the value, for example, for a , one uses Eq. (17) to determine an appropriate value for the coefficient b . Once a and b are known, one then uses the methods described in Section 3 to invert the GIC and the magnetic field data to an optimal ground conductivity model.

In conclusion, we argue that the methods described above

can be used to convert GIC, magnetic field and geoelectric field observations to system parameters and a ground conductivity model that enable an optimal GIC modeling. The usage of the methods was demonstrated by means of application to actual GIC and ground magnetic field observations carried out in southern Finland. It was seen that optimal site-dependent system parameters and ground conductivity structure can be obtained using a time series comprising only 8 days worth of data. Also, the demonstration indicated that although in an ideal case the magnetic field data used should be obtained from the immediate vicinity of the GIC observation site, some spatial separation (200–300 km) between the GIC and the magnetometer sites can be tolerated. Obviously, the introduced methods can be used to extract information from any technological system experiencing GIC and about any geographical region having an approximately 1D ground conductivity structure. Furthermore, from a less applications-oriented viewpoint, it was shown that GIC observations can provide valuable additional information for MT-based studies of subsurface geological structures.

Acknowledgments. Gasum Oy has contributed to studies on geomagnetically induced currents in the Finnish natural gas pipeline for about 25 years. We would especially like to thank Juha Vainikka and Matti Pitkänen for a continuous interest in our work. The IMAGE magnetometer array is an international project headed by the Finnish Meteorological Institute (<http://www.ava.fmi.fi/image/>). We also wish to thank both referees for their valuable comments and constructive criticism that helped to greatly enhance the quality of our work.

References

- Boteler, D. H., R. J. Pirjola, and H. Nevanlinna, The Effects of Geomagnetic Disturbances on Electrical Systems at the Earths Surface, *Adv. Space Res.*, **22**, 17, 1998.
- Brasse, H. and A. Junge, The influence of geomagnetic variations on pipelines and an application for large-scale magnetotelluric depth sounding, *Journal of Geophysics*, **55**, 31–36, 1984.
- Cagniard, L., Basic theory of the magneto-telluric method of geophysical prospecting, *Geophysics*, **18** (3), 605–635, 1953.
- Constable, S., R. Parker, and C. Constable, Occam’s inversion: A practical algorithm for generating smooth models from electromagnetic sounding data, *Geophysics*, **52**(3), 289–300, 1987.
- Dmitriev, V. and M. Berdichevsky, The fundamental model of magnetotelluric sounding, *IEEE Proc.*, **67**, 1034, 1979.
- Egbert, G. and J. Booker, Robust estimation of geomagnetic transfer functions, *Geophys. J. R. Astr. Soc.*, **87**, 173–194, 1986.
- Eisel, M. and G. Egbert, On the stability of magnetotelluric transfer function estimates and on the reliability of their variances, *Geophys. J. Int.*, **144**, 65–82, 2001.
- Hejda, P. and J. Bochnicek, Geomagnetically induced pipe-to-soil voltages in the Czech oil pipelines during October–November 2003, *Ann. Geophys.*, **23**, 3089–3093, SRef-ID: 1432-0576/ag/2005-23-3089, 2005.
- Koen, J., Geomagnetically induced currents in the Southern African electricity transmission network, PhD thesis, University of Cape Town, 2002.
- Korja, T., M. Engels, A. A. Zhamaletdinov, A. A. Kovtun, N. A. Palshin, M. Yu. Smirnov, A. Tokarev, V. E. Asming, L. L. Vanyan, I. L. Vardaniants, and the BEAR Working Group, Crustal conductivity in Fennoscandia—a compilation of a database on crustal conductance in the Fennoscandian Shield, *Earth Planets Space*, **54**, 535–558, 2002.
- Lehtinen, M. and R. Pirjola, Currents produced in earthed conductor networks by geomagnetically-induced electric fields, *Ann. Geophys.*, **3**(4), 479–484, 1985.
- McKay, A., Geoelectric Fields and Geomagnetically Induced Currents in the United Kingdom, PhD thesis, University of Edinburgh, 2003.
- Pal’shin, N. A., The Method of Deep Magnetotelluric Soundings Using Electric Currents Induced in Operating Power Lines: the Case Study

- of the Loviisa-Nurmijärvi Power Line, *Izvestiya, Physics of the Solid Earth*, **34**, No. 1, Scientific Communications, 72–75, Translated from *Fizika Zemli*, No. 1, 1998, pp. 80–83, 1998.
- Pirjola, R., Geomagnetic effects on Ground-Based Technological Systems, *Review of Radio Science*, URSI, 473, 2002.
- Press, W. H., S. A. Teukolsky, W. T. Vetterling, and B. P. Flannery, *Numerical recipes in FORTRAN: the art of scientific computing*, 2nd ed., Cambridge University Press, Cambridge, 1992.
- Pulkkinen, A., R. Pirjola, D. Boteler, A. Viljanen, and I. Yegorov, Modelling of space weather effects on pipelines, *J. Appl. Geophys.*, **48**, 233–256, 2001a.
- Pulkkinen, A., A. Viljanen, K. Pajunpää, and R. Pirjola, Recordings and occurrence of geomagnetically induced currents in the Finnish natural gas pipeline network, *J. Appl. Geophys.*, **48**, 219–231, 2001b.
- Pulkkinen, A. and M. Engels, The role of 3D geomagnetic induction in the determination of the ionospheric currents from the ground geomagnetic data, *Ann. Geophys.*, **23**, 909–917, 2005.
- Pulkkinen, A., A. Klimas, D. Vassiliadis, V. Uritsky, and E. Tanskanen, Spatiotemporal scaling properties of the ground geomagnetic field variations, *J. Geophys. Res.*, **111**, A03305, doi:10.1029/2005JA011294, 2006a.
- Pulkkinen, A., A. Viljanen, and R. Pirjola, Estimation of geomagnetically induced current levels from different input data, *Space Weather*, **4**, S08005, doi:10.1029/2006SW000229, 2006b.
- Simpson, F. and K. Bahr, *Practical Magnetotellurics*, Cambridge University Press, 2005.
- Tikhonov, A. N., On determining electrical characteristics of the deep layers of the Earth's crust, *Dokl. Akad. Nauk. SSSR*, **73**, 295–297, 1950.
- Utada, H., T. Koyama, H. Shimizu, and A. D. Chave, A semi-global reference model for electrical conductivity in the mid-mantle beneath the north Pacific region, *Geophys. Res. Lett.*, **30**(4), 1194, doi:10.1029/2002GL016092, 2003.
- Viljanen, A., R. Pirjola, and O. Amm, Magnetotelluric source effect due to 3D ionospheric current systems using the complex image method for 1D conductivity structures, *Earth Planets Space*, **51**, 933–945, 1999.
- Viljanen, A., A. Pulkkinen, O. Amm, R. Pirjola, T. Korja, and Bear Working Group, Fast computation of the geoelectric field using the method of elementary current systems, *Ann. Geophys.*, **22**, 101–113, 2004.
- Viljanen, A., A. Pulkkinen, R. Pirjola, K. Pajunpää, P. Posio, and A. Koistinen, Recordings of geomagnetically induced currents and a nowcasting service of the Finnish natural gas pipeline system, *Space Weather*, **4**, S10004, doi:10.1029/2006SW000234, 2006.
- Weidelt, P., The Inverse Problem of Geomagnetic Induction, *Z. Geophys.*, **38**, 257–289, 1972.

A. Pulkkinen (e-mail: antti.a.pulkkinen@nasa.gov), R. Pirjola, and A. Viljanen